



**BRNO UNIVERSITY OF TECHNOLOGY**

VYSOKÉ UČENÍ TECHNICKÉ V BRNĚ

**FACULTY OF MECHANICAL ENGINEERING**

FAKULTA STROJNÍHO INŽENÝRSTVÍ

**INSTITUTE OF MATERIALS SCIENCE AND ENGINEERING**

ÚSTAV MATERIÁLOVÝCH VĚD A INŽENÝRSTVÍ

**SHORT CRACK GROWTH IN MATERIALS  
FOR HIGH TEMPERATURE APPLICATIONS**

ŠÍŘENÍ KRÁTKÝCH TRHLIN V MATERIÁLECH PRO VYSOKÉ TEPLoty

**DOCTORAL THESIS – SHORTENED VERSION**

DIZERTAČNÍ PRÁCE

**AUTHOR**  
AUTOR PRÁCE

Ing. Veronika Mazánová

**SUPERVISOR**  
ŠKOLITEL

prof. RNDr. Jaroslav Polák, DrSc. dr.h.c.

**BRNO 2019**

**Key words:** low cycle fatigue, austenitic stainless steel, damage mechanisms, fatigue crack initiation, PSBs, PSMs, natural short crack growth, fracture mechanics, short crack growth law, fatigue life, high temperature oxidation, SEM, EBSD, STEM

**Klíčová slova:** nízkocyklová únava, austenitická nerezová ocel, mechanismy poškození, iniciace únavové trhliny, persistentní skluzové pásy (PSBs), persistentní skluzové stopy (PSMs), růst přirozených krátkých trhlin, lomová mechanika, zákon růstu krátkých trhlin, únavový život, oxidace za vysokých teplot, rastrovací elektronová mikroskopie (SEM), EBSD, rastrovací transmisní elektronová mikroskopie (STEM)

The thesis is stored at the Science and Research department  
Faculty of Mechanical Engineering, Brno University of Technology  
Technická 2896/2, 61662 Brno, Czech Republic

Veronika Mazánová ©, 2019

Institute of Materials Science and Engineering  
Faculty of Mechanical Engineering  
Brno University of Technology

[mazanova@ipm.cz](mailto:mazanova@ipm.cz)

ISBN 80-214-XXX  
ISSN 1213-419

## Contents

<b>1. INTRODUCTION .....</b>	<b>- 2 -</b>
<b>2. AIMS OF THE WORK .....</b>	<b>- 3 -</b>
<b>3. EXPERIMENTS .....</b>	<b>- 3 -</b>
3.1. Austenitic stainless steel – Sanicro 25 .....	- 3 -
3.2. Mechanical testing .....	- 5 -
3.2.1. Specimens .....	- 5 -
3.2.2. Cyclic loading .....	- 6 -
3.3. Microscopic observation .....	- 6 -
3.3.1. Light microscopy .....	- 6 -
3.3.2. Scanning electron microscopy .....	- 7 -
3.3.3. Transmission electron microscopy .....	- 8 -
<b>4. SELECTED RESULTS .....</b>	<b>- 8 -</b>
4.1. Fatigue damage at room temperature .....	- 8 -
4.1.1. Natural fatigue crack initiation sites .....	- 8 -
4.1.2. Crack growth of natural cracks .....	- 12 -
4.1.3. Crack growth kinetics of short natural cracks and fatigue life .....	- 12 -
4.2. Fatigue damage at temperature of 700 °C .....	- 17 -
4.2.1. Grain boundary oxidation and crack initiation .....	- 17 -
4.2.2. Crack growth under environmental conditions .....	- 19 -
<b>5. CONCLUSIONS .....</b>	<b>- 20 -</b>
<b>6. REFERENCES .....</b>	<b>- 22 -</b>
<b>7. Veronika Mazánová - List of selected publications .....</b>	<b>- 26 -</b>
<b>8. Curriculum Vitae .....</b>	<b>- 27 -</b>
<b>Abstract .....</b>	<b>- 28 -</b>

# 1. INTRODUCTION

The demands on the increase of the material properties from the side of the industry force the materials research highly forward. In the case of new generation of coal-fired power plants the increase of the material properties such as creep strength, high-temperature strength and high-temperature corrosion resistance are essential material features leading to the increase of the power plant heat efficiency higher than 50 %. Moreover, the environmental impact in the form of carbon dioxide generated by combustion processes can be decrease by more than 15 % compared with modern power plants [1]. Such a material can be newly developed austenitic stainless Sanicro 25 steel. It is advanced high strength heat-resistant material primarily designed for service in high temperature corrosive environments [1]. However, based on its excellent properties, there is an expectation for its wider utilization also in other industrial applications.

During the service conditions variable forces or rapidly changing temperatures lead to the production of alternating stresses and strains, preferably in critical locations. Repeated alternating stresses introduce fatigue damage and lead to initiation of fatigue cracks, their propagation, and fracture. Due to service conditions, both high and room temperature fatigue can result in failure of structural components. Therefore, not only the deformation mechanisms taking place during the cyclic loading but also the detailed knowledge of the damage evolution leading to final fracture is useful in preventing catastrophic failures. The knowledge of the weaknesses of the material can help to its future improvement.

Numerous studies of the fatigue process in materials revealed [2] principal stages in the fatigue life, initiation of fatigue cracks and their propagation. In elastoplastic cyclic loading resulting in low cycle fatigue failure, the highest importance represents the initiation of fatigue cracks and growth of short cracks because they determine the fatigue life. The early study of fatigue crack initiation started in the beginning of the last century (see the pioneering work of Ewing and Humfrey [3]), but the intensive study of both crack initiation and short crack growth in a number of polycrystalline materials with the aim to document the advancement of fatigue damage and damaging mechanisms started much later (see the review [4; 5]).

Complex conditions in real service need thorough studies of deformation and damage mechanisms during both unidirectional and cyclic loading. The microstructural features that lead to the cyclic strain localization and the initiation of fatigue cracks at room temperature and at elevated service temperature differ significantly [6]. At high temperatures, the early fatigue damage is not only affected by the type of loading [7; 8], but also by the environmental effects causing grain boundary oxidation and cracking [9; 10].

The purpose of this work is to reveal the details of the low-cycle fatigue crack initiation and natural short crack growth both at room temperature and at a temperature of 700°C in Sanicro 25 and to provide the insights into the mechanisms determining the fatigue life of this austenitic steel. Advanced experimental tools are used to investigate the microstructural changes leading to the early stages of fatigue crack initiation and growth. The results are discussed in relation to the proposed models of fatigue crack initiation and estimation of residual fatigue life. The role of high temperature is discussed in relation to the overall fatigue life of the alloy.

## **2. AIMS OF THE WORK**

This thesis is focused on the fatigue damage mechanisms taking place during the low cycle fatigue of recently developed austenitic stainless Sanicro 25 steel used in power generation industry. The damage mechanisms are studied during the cyclic straining at both room and elevated temperatures. Special emphasis is put on the investigation of the fatigue crack initiation since in the low cycle fatigue regime the fatigue crack initiation period represents the significant part of the fatigue life. The parameters describing the short crack growth were evaluated for the samples cycled at room temperature. Several minor goals were specified to be accomplished within the study as listed below:

- Characterization of the initial state of the material.
- The analysis of the fatigue crack initiation taking place at both ambient and elevated temperatures. Discussion of the role of the environment in the crack nucleation mechanism.
- The investigation of the crack initiation sites leading to the growth of the major cracks. Discussion of the microstructural changes of the material due to the cyclic loading in relation to the early stages of the crack nucleation.
- Study of the short crack growth mechanisms in the material subjected tension-compression loading at room temperature as well as at elevated temperature.
- Measurement of the crack growth rates on the samples subjected to cycling with constant total strain amplitudes at room temperature.
- The evaluation of the characteristic parameters, which determine the rate of fatigue crack growth in relation to the different loading rates. The estimation of the residual fatigue life.

## **3. EXPERIMENTS**

### **3.1. Austenitic stainless steel - Sanicro 25**

Austenitic stainless steel of the grade UNS S31035, and with the trade name Sanicro 25, was produced by Sandvik, Sweden. The chemical composition of the material in the as-received condition (in wt%) is listed in Table 3.1.1. The material was delivered in the form of hot rolled cylindrical rods of 150 mm in diameter. The specimens for the mechanical testing were machined parallel to the rod axis. After the production of their crude shape, the specimens were annealed at 1200 °C for one hour and cooled in the air.

	Fe	Ni	Cr	W	Cu	Co	Nb	Mn	N	Si	C
This work	42.9	25.0	22.5	3.6	3.0	1.5	0.5	0.5	0.23	0.2	0.1
Producer	Bal.	23.5 –	21.5 –	2.0 –	2.0 –	1.0 –	0.3 –	0.6	0.15 –	0.4	0.04 –
Min/Max		26.6	23.5	4.0	3.5	2.0	0.6	Max	0.30	Max	0.1

Table 3.1.1: The nominal composition of studied Sanicro 25 highly alloyed austenitic stainless steel (in wt%). Composition of steel studied in this work is compared with the composition guaranteed by the producer [1].

Microstructure characterization of initial state of the material before the loading was performed by SEM

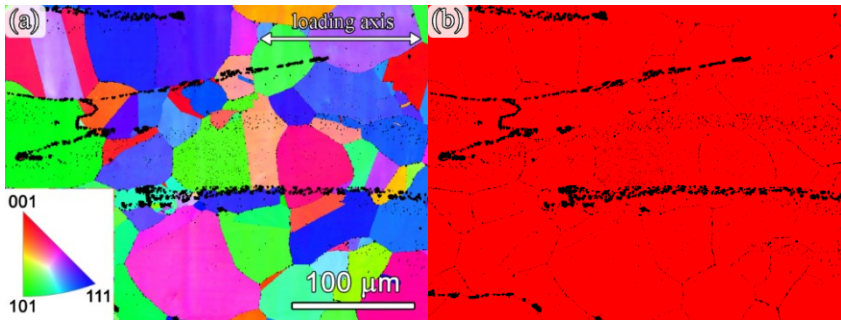


Figure 3.1.1: Structure of the Sanicro 25 after annealing; a) grain orientation relative to the loading axis obtained by EBSD; b) EBSD micrograph of phases (austenite — red, primary precipitates — black).

The orientation of individual grains is random. EBSD grain orientation analysis shows the presence of multiple annealing twin boundaries in the structure. Phase analysis in Fig. 3.1.1b shows that the matrix is composed only from austenitic grains. Nevertheless, the primary particles of Z-phase are present in the material as well (shown as black color in Fig. 3.1.1b) [12; 13].

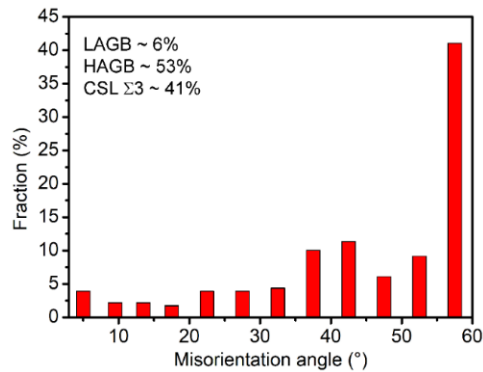


Figure 3.1.2: Statistics of the fraction of grain boundaries with particular misorientation angle in the initial state observed by EBSD. Low angle grain boundaries (LAGB) represent approx. 6%, high angle grain boundaries (HAGB) approx. 53% and twin boundaries ( $\Sigma 3$ ) approx. 41% of the total number of investigated grain boundaries.

From the total number of analyzed grain boundaries the fraction of observed grain boundaries with particular misorientation angle at the interface was determined by EBSD. Results are shown in Fig. 3.1.2. It is evident, that the high angle grain boundaries (HAGB) significantly predominate when compared to low angle grain boundaries (LAGB).  $\Sigma 3$  twin boundaries with misorientation angle of about  $60^\circ$  with respect to the  $\{1\ 1\ 1\}$ -type of planes represent fraction of about 41% of all detected boundaries. Statistically, this means that approx. 80% of grains contain one twin boundary at maximum what is in a good agreement with the initial structure shown in Fig. 3.1.1a. Other special CSL type interfaces except for the twin boundaries represent only about 5%, what means that randomly oriented HAGB interfaces predominate.

The material tensile and fatigue parameters are listed in Tab. 3.1.2.

$T$ (°C)	$E$ (GPa)	$R_{p0.2}$ (MPa)	$R_m$ (MPa)	$A$ (%)	$K'$ (MPa)	$n'$	$\varepsilon_f'$	$c$	$\sigma_f'$ (MPa)	$b$ (MPa)
20	200	320	740	59	1006	0.186	0.700	-0.526	962	-0.100
700	130	190	487	51	1243	0.181	0.090	-0.539	797	-0.090

Table 3.1.2: Tensile and low cycle fatigue parameters of Sanicro 25 at two temperatures. (Taken from [14])

## 3.2. Mechanical testing

### 3.2.1. Specimens

Solid cylindrical specimens with the diameter of 8 mm and gauge length of 12 mm were used for loading at room temperature (see Fig. 3.2.1a). The axis of the specimen is parallel to the axis of the cylindrical rod. Shallow notch of depth 0.4 mm was ground in the middle of the gauge length to facilitate the observation of the surface evolution and cracks. The theoretical stress concentration factor of the notch  $K_t$  was determined by finite element method (FEM) using numerical program ANSYS. Fig. 3.2.1. shows the detail of the notch and the result of elastic strain distribution. The value of theoretical stress concentrator factor  $K_t = 1.185$  is small enough to have only minor impact on the crack nucleation in other parts of the specimen but high enough to initiate the major crack in the observed area of the shallow notch. The area of the shallow notch was polished by soft 8" SiC grinding paper (EuropeanFEPA Grit Rating 1200). Then the surface was electrolytically polished and the chemical composition of the used electrolyte was 500 ml of ethanol, 7.5 ml of nitric acid, and 25 ml of perchloric acid.

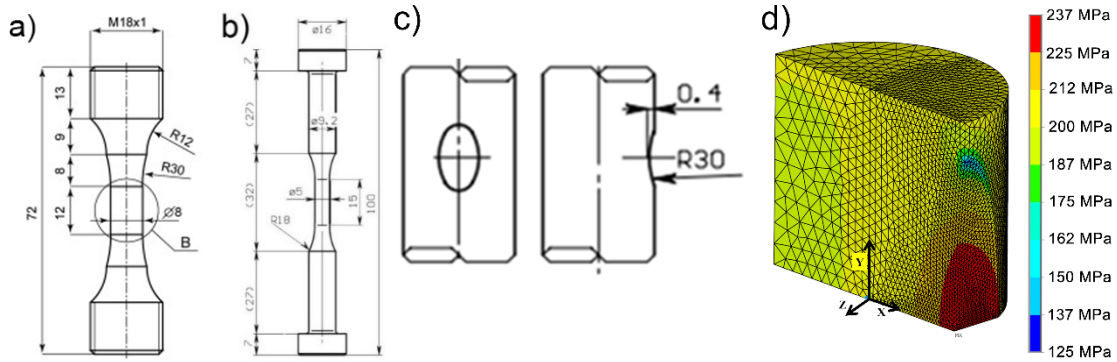


Figure 3.2.1: Geometry of the specimens: a) specimen for cyclic loading at room temperature and b) specimen for cyclic loading at high temperature. c) Geometry of the shallow notch and d) the stress analysis of the notch effect under static uniaxial loading using ANSYS in the specimen axis direction  $Y$  (loading direction).

In the case of high temperature loading the solid cylindrical specimens with the diameter of 6 mm and the gage length of 15 mm were used (see Fig. 3.2.1b). To eliminate the effect of the surface roughness on the fatigue and to facilitate the observation of the surface relief evolution, the area corresponding to the gage length was mechanically grinded and electrolytically polished in the same manner as samples used for testing at room temperature.

### 3.2.2. Cyclic loading

All tests were carried out using servo-hydraulic tension-compression computer-controlled MTS testing machines MTS 810. The tests were performed under fully reversed ( $R_\epsilon = -1$ ) strain controlled cycling with constant strain rate. Temperature of the samples was controlled by thermocouples in the range  $\pm 2^\circ\text{C}$ . Stress and strain were recorded in regular intervals during cycling. During one hysteresis loop, 400 data-points containing information about the stress and the strain levels were taken. Stress and strain amplitudes were derived from the hysteresis loops acquired during the cycling. Plastic strain amplitude was determined as the half-width of the hysteresis loop at mean stress.

Cycling straining at room temperature was conducted under strain controlled cyclic loading with constant strain rate of  $5 \times 10^{-3} \text{ s}^{-1}$  and the constant total strain amplitudes  $\epsilon_a$  in the range of  $(2.5 - 7.0) \times 10^{-3}$ . Mechanical grips held at the constant temperature by water cooling system were used. Force was measured by a load cell. The displacement and the strain during loading were controlled and determined by uniaxial extensometer having the 8 mm base between the knife-edges. To measure the crack growth, the area of the notch was regularly observed. In order to analyze the crack increment the fatigue test was interrupted at a chosen number of cycles. The specimen was kept in tension (at zero strain) to ensure open cracks during the image acquisition.

Continuous isothermal tests were carried out at the temperature of  $700^\circ\text{C}$ . High temperature hydraulic grips and a split three-zone resistance furnace were used to keep the desired temperature with minimum temperature gradient across the gage length. Specimen temperature was monitored by three thermocouples (two located on both heads of the sample and the one monitoring the temperature in the middle of the gage length). Again, the mechanical grips held at the constant temperature by water cooling system were used. Fully reversed cyclic loading with the constant total strain amplitude of  $5.0 \times 10^{-3}$  and the constant strain rate of  $2 \times 10^{-3} \text{ s}^{-1}$  was applied. Strain was measured and controlled using high temperature axial extensometer having long ceramic rods and 12 mm base. Specimen was heated to the high temperature (around 30 minutes) and after a full stabilization (around 1 hour) the cyclic straining was started to minimize the high-temperature exposure of the specimen before cycling.

## 3.3. Microscopic observation

### 3.3.1. Light microscopy

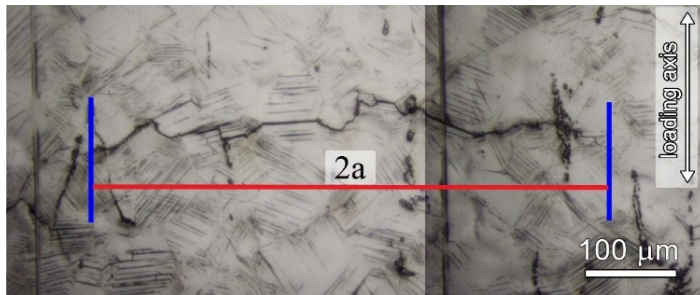


*Figure 3.3.1: Surface crack length  $2a$  (red line) of a semicircular crack in the direction perpendicular to the loading axis.*

Fatigue crack initiation and growth was studied on specimens with polished gage section using long focal distance capable light microscope (LM) Navitar equipped with Olympus DP 70 high resolution camera. The images were acquired with the resolution of  $0.15 \mu\text{m}$  corresponding to 1 pixel. Surface cracks up to 2 mm of surface length were studied during cyclic loading. Images of the studied area were acquired regularly and the crack length was measured directly. To facilitate the observation of

the notch area the periodic net of straight shallow lines was ground on the surface by the razor. The spacing of 0.5 mm between the lines was used. The test was stopped after the one of the cracks achieved the surface length more than 2 mm within the observed area the test was stopped. Hence, the lengths of about five largest cracks within the observed area were measured. The growth of these particular selected cracks was analyzed backwards from the previously stored images. Since the crack shapes in



austenitic steel are assumed to be approximately semicircular [15; 16], the crack length  $a$  in the bulk was characterized by the half of its surface length (i.e. the distance between the crack tips on the specimen surface) projected on a plane perpendicular to the loading axis as marked by red line in Fig. 3.3.1. The crack growth rate was then defined as the increment of the crack length,  $\Delta a$ , in the number of the cycles.

### 3.3.2. Scanning electron microscopy

The surface of the selected specimen for further investigation was inspected in detail using dual-beam Lyra 3 XMU FEG-SEM (Tescan) equipped with the focused ion beam (FIB), backscattered electron (BSE), electron backscatter diffraction (EBSD) and X-Max80 energy dispersive X-ray spectroscopy (EDS) detectors all produced by the Oxford Instruments and operated with the Aztec control system.

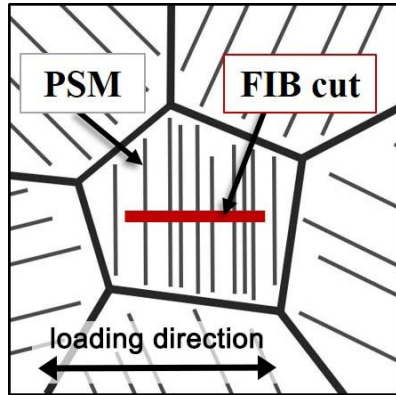


Figure 3.3.2: Schematic position of the FIB cut in the grain perpendicular to the persistent slip markings.

The mechanism of the initiation of the cracks was studied using technique of coupled FIB nanofabrication and EBSD analysis. In the case of loading at high temperatures the EDS analysis was also used to study the changes in the composition and to characterize the oxidation behaviour of the material. Specimens in selected stages of the fatigue life or at the fracture were investigated. In order to reveal the shape of the surface relief and the shape of the initiated crack in the third dimension, the grains with PSMs running perpendicular to the specimen axis were chosen. Lamellae perpendicular to the direction of PSMs were produced using FIB. Fig. 3.3.2 schematically shows the position of the lamella situated approximately in the center of the grain. The area of the interest was documented using FESEM, and later selected area of the grain with several PSMs was covered with platinum. Very thin platinum layer was first deposited using electron bombardment and later a layer of about 1.5 - 2  $\mu\text{m}$  in thickness was deposited using ion bombardment. FIB was used to produce rectangular craters from one side and later from both sides of the future lamella. However, only one lamella could be prepared using FIB from the grain containing PSMs and subsequently observed in transmission electron microscope (TEM). Lamella was further completely separated from the grain, mounted to the supporting copper grid, and subjected to further thinning. Both surfaces of the lamella were finally thinned with ions using low acceleration voltage of 5 kV and current of 300 pA in order to remove or minimize the damage caused by previous steps.

Thin TEM lamellae prepared by FIB were used also to study the oxidation of grain boundaries during the cycling at high temperature. The lamellae were extracted at the position where the grain boundary was roughly oxidized. The grain boundary was oriented approximately perpendicular to the loading axis.

After the cycling, the relation between the structure of the material and the crack growth path was studied using the EBSD. The EBSD was done using acceleration voltage of 20 kV and the average spot spacing up to 1  $\mu\text{m}$ . The crystallographic orientation of the grains along the crack was analysed. The obtained Euler rotation angles of individual grains were used to define orientation of primary slip planes  $\{111\}$ . Subsequently their projection to the planes described in the basic cartesian coordinate system (XYZ) was analysed by software developed in Matlab at the IPM CAS by Roman Gröger.

### 3.3.3. Transmission electron microscopy

Thin foils suitable for TEM observations could be inspected either in FESEM to document surface relief or directly in JEOL JEM-2100 F TEM (Jeol Ltd., Tokyo, Japan) equipped with FEG (Field Emission Gun) electron source. To visualize crystal defects such as dislocations, the diffraction contrast imaging in STEM (scanning transmission electron microscopy) was used. Both the bright and dark field detectors were utilized to inspect the crystal either along low index zone axes or in several different two-beam diffraction conditions. When inspecting arrangement of dislocation structures, the images were taken in at least four diffraction conditions to get all possible geometrical information about the crystal, slip planes and slip directions. The zero contrast invisibility rule known also as “*g.b*” rule was used to determine the Burgers vectors and the type and character of dislocations. To image different phases, electrons inelastically scattered to high angles were collected to annular dark field detector to obtain Z-contrast which is sensitive and proportional to atomic number ( $\sim Z^2$ ) of elements.

The TEM lamellae were fixed in the TEM holder with the loading direction aligned with the respect to the holder axis. The goal was to know the orientation of investigated crystal relative to the macroscopic loading axis during the observations. Diffraction patterns and Kikuchi lines were used to determine the crystallographic orientation of the stress axis in individual grains. If not stated otherwise, the Miller's indexes were permuted so that the strain axis vector lay in or on the border of the basic stereographic triangle defined by the apexes [001], [011], [ $\bar{1}11$ ].

## 4. SELECTED RESULTS

### 4.1. Fatigue damage at room temperature

#### 4.1.1. Natural fatigue crack initiation sites

Preferential mechanisms and sites of the fatigue crack initiation were closely studied in specimens cyclically loaded with different total strain amplitudes. The fractions of all studied possible sites, where the crack initiation could be identified, i.e., in PSMs, PSMs along the TBs, GBs and close to inclusions were evaluated. Graphs in Fig. 4.1.1 show the percentage of the cracks initiated in 4 locations during

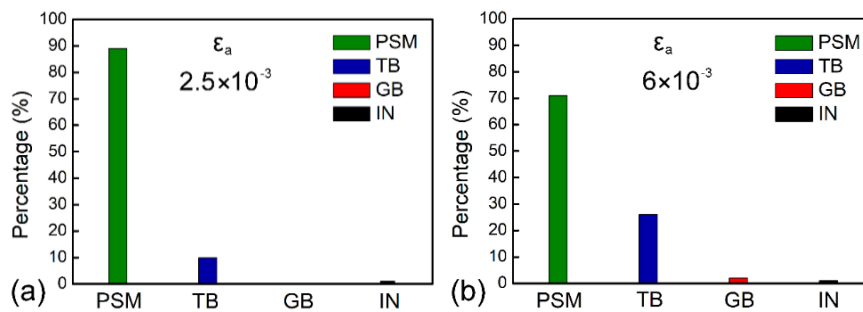


Figure 4.1.1: Fatigue crack initiation type for low ( $2.5 \times 10^{-3}$ ) and high ( $6 \times 10^{-3}$ ) total strain amplitude. PSM - persistent slip marking (PSB in the grain), TB - twin boundary (PSM at the TB), GB - grain boundary, IN – inclusion.

As can be seen, no crack initiation at the GB as the result of the slip band impingement on the GB was documented in the case of small strain amplitude cycling. All initiated cracks observed close to grain boundaries were initiated as the result of enhanced slip activity and development of PSMs in GBs. Unlike that, small fraction of cracks initiated at GBs (of about 2%) was observed in the case of high strain amplitude loading. The inclusions played only a minor role in crack initiation in cycling with both low and high strain amplitude. Only approximately

1% of all studied cracks initiated from or were passing through inclusions. Twin boundaries were found to be often associated with the appearance of PSMs as reported in previous section. By comparing statistics in Fig. 4.1.1, it is apparent that the effect of TBs on the formation of PSMs and subsequently on the crack initiation along the TBs increases with increasing applied strain amplitude from 10% to 30%. Nevertheless, crack initiation along the PSMs developed within the grains plays a predominant role in both low and high strain amplitude loading. Because the initiation along the TB is associated with the production of PSM adjacent to TB, we can conclude that PSMs are the principal sites where the fatigue crack initiation was observed in both low and high strain amplitude cyclic loading.

a) Persistent slip markings within the surface grains

Later in the 70<sup>th</sup> and 80<sup>th</sup> of the last century the role of internal dislocation structure in the form of persistent slip bands was found to be the essential feature leading to the formation of the surface relief [17-19]. In the case of pure materials with high SFE such as Cu or Ni the cyclic plastic strain is localized into the narrow persistent slip bands with dislocation rich walls and dislocation free channels [20; 21]. The ladder-like structures follow exactly the trace of the primary slip plane. Surface relief in the form of PSMs anticipates the crack initiation.

Micrograph in Fig. 4.1.2a shows typical relief of surface grain after fatigue where several well-developed parallel PSMs A-E are present. PSMs consist of one or more extrusions and parallel intrusions. Nanofabricated FIB trench perpendicular to the PSM A (see Fig. 4.1.2b) shows the presence of two extruded hills (extrusions) and depressed material (intrusion) in between them is evident. Here, from the tip of the intrusion, Stage I fatigue crack was found to initiate. According to Hunsche and Neumann [22] the crack can be distinguished from the intrusion by the vortex angle. Whereas the vortex angle of crack is zero, the intrusion has a non-zero vortex angle. The relief of extrusions and intrusion is not smooth; some alternating small extrusions/intrusions can be found even within individual large extrusions as was previously found e.g. in 316L steel [4].

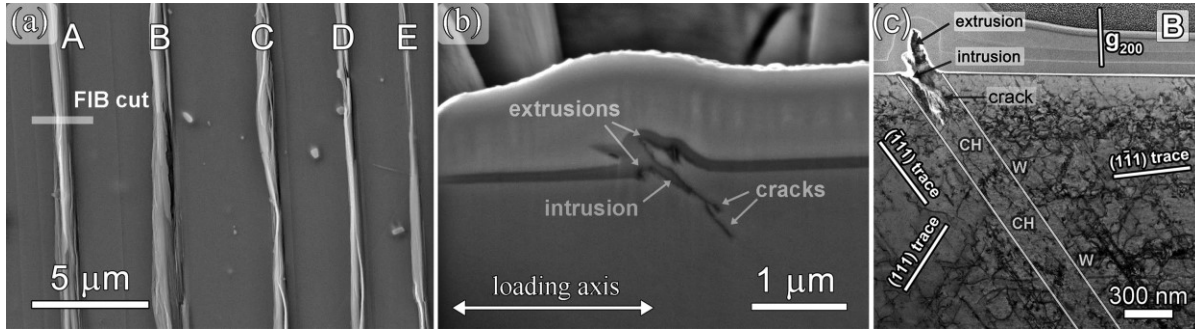


*Figure 4.1.2: SE micrograph of the specimen cycled with total strain amplitude  $\epsilon_a = 0.35\%$ ; (a) specimen surface with 5 parallel PSMs; (b) the profile of the PSM a in the location marked in (a) as “FIB cut” showing extrusions, intrusion, and cracks starting from the tip of the intrusion. (c) Detailed image of the internal dislocation structure and of the persistent slip marking showing the persistent slip marking consisting of extrusion and intrusion and a crack starting from the tip of the intrusion. The specimen was tested with total strain amplitude  $\epsilon_a = 0.25\%$ ;*

Close inspection of the foils produced from the surface grains of Sanicro 25 steel shows that the dislocation structure of the PSBs under the PSMs does not clearly differ from the dislocation structure of the matrix. Generally, the dislocation density within the PSBs is lower than in the matrix, and definitely, dislocations from secondary slip systems running through the matrix were absent in the PSBs. The ladder-like dislocation structure is found only occasionally as shown in Fig. 4.1.2c. Our observations agree with the studies performed on 316L steel [23-25] where the low SFE leads to the increased planar glide of dislocation. In summary, two important differences of PSB structure from the matrix structure are apparent: (i) absence of dislocations from secondary slip systems, and (ii) low

dislocation density in some areas of PSBs. We can thus characterize the dislocation structure as irregular alternations of the volumes rich and poor in dislocations.

Several models were proposed to explain the formation of PSMs and crack initiation [26-30]. Only the EGM model [29] and Polák's model [30] consider the role of the point defects within the PSB. The EGM model [29] predicts formation of vacancies in the walls of PSBs. Vacancies arise because of dislocation interactions in the dislocation-rich walls. In the case vacancies cannot migrate, they accumulate in the walls and the volume of PSB increases. Extra volume results in internal compressive stress and plastic relaxation of this stress in the direction of the Burgers vector produces extrusions where PSBs egress on the surface. The 'intrusions' develop as a consequence of the previously formed extrusions and are in fact embryonic Stage I shear cracks. Polák's model [30] is based on the EGM assumption of the continuous production of point defects due to dislocation interactions in locations of cyclic plastic strain localization. Contrary to the EGM model, only point defects produced in the channels of the PSB can escape from PSB to the matrix and are systematically annihilated at edge dislocations in the matrix. Majority of them are absorbed at dislocations close to the PSB/matrix boundary. It results in systematic transfer of matter from the matrix to the PSB. The plastic relaxation of the internal stresses within the PSB in the direction of Burgers vector leads to the formation of extrusion and intrusion pairs at the surface (see Fig. 4.1.2). The only essential condition for the formation of PSMs is the localization of the cyclic plastic strain in the bands of cyclic slip (PSBs) with alternating dislocation rich and dislocation poor volumes. The Stage I crack nucleate from the tip of the intrusion. According to Polák's model the crack initiation could appear on both sides of the extrusion since the intrusions can form at both interfaces PSB/matrix what agrees with our experimental results. However, based on the conclusions done on fatigued 316L steel at room temperature by Man et al. [4] the intrusions start more frequently on the extrusion side where the active slip plane inclines to the surface at an acute angle.

#### b) Twin boundaries and grain boundaries

The transition from trans- to intercrystalline crack initiation increases with increasing applied total strain amplitude i.e. with increased plastic strain amplitude. The TBs were observed to be the second preferential site of fatigue crack initiation since they promote early cyclic slip localization and PSB formation [31; 32]. Consequently, it was demonstrated several times that the cracking of TBs plays an important role in specimens fatigued with low strain amplitudes [16]. However, their important role was found in 316L steel also at intermediate and high strain amplitudes [33; 34]. Based on our observations the relative frequency of TB cracking increases with increasing strain amplitude (see Fig. 4.1.1).

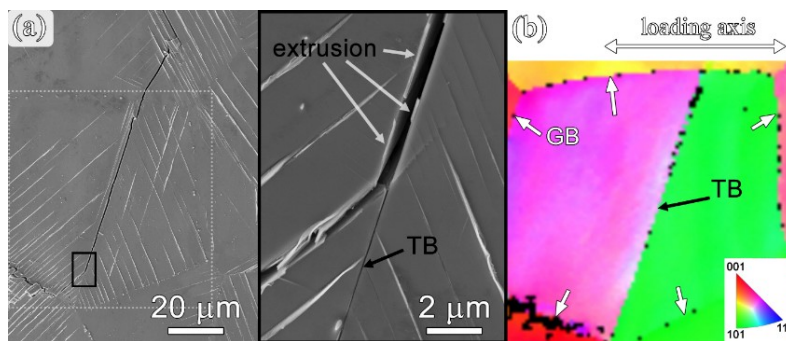


*Figure 4.1.3: Crack initiation along the twin boundary: (a) SE micrograph of the specimen surface with a crack initiated in the TB along the PSM (see the detail highlighted by black inset); (b) EBSD image in the loading direction of the area selected by dashed rectangle in Fig. 4.1.3a*

Most of the TB cracking was observed to be related to the appearance of PSB emerging at the surface along the TB. The role of TBs in fatigue crack initiation have been studied in various simple metals [31; 35] as well as in structural materials [16; 33]. The characteristic bands of the localized cyclic plastic deformation (PSBs) running parallel to the TBs were often reported for copper [32; 36]. Our observations reveal the surface relief in the form of extrusions and intrusion. Since we have

observed the extrusions along the surface cracks running along TBs (see Fig. 4.1.3) we can conclude that the cracking of TBs was pronounced by the appearance of parallel PSBs.

The most relevant theoretical model of crack nucleation along the TB was proposed by Neumann et al. [35; 37]. They analysed the elastic anisotropy of the TB pair and stress concentration near the emerging TBs. They concluded that the effective resolved shear stresses near the TB due to the elastic anisotropy of surrounding twins locally enhances the plasticity along the TB and intensify the formation of PSB/PSM since the TB is parallel with  $\{111\}$  slip plane. The model was slightly modified by Blochwitz et al. [16; 33; 38] for intermediate and high strain amplitudes considering the elasto-plastic solution. Their results are consistent with the observations of Neumann. This is in agreement with our observations which confirmed the role of TB both in low and high strain amplitude cycling. The probability that the nucleated crack along the TB would develop into the dominant crack is enhanced in the case of high strain amplitudes (see Fig. 4.1.1).

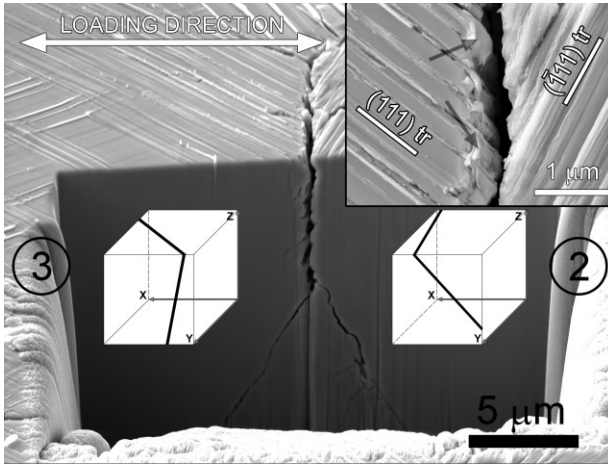


Figure 4.1.4: SE image of the area containing FIB cross section plane oriented perpendicular to the cracked GB. The specimen was cycled with  $\epsilon_a = 6 \times 10^{-3}$  ( $\epsilon_{ap} (N_f/2) = 4 \times 10^{-3}$ ). The image was taken with the  $35^\circ$  tilt correction. The insets show the orientation of the primary slip planes in individual grains. Detail in the rectangle shows the PSBs emerging at GB and PSMs arise here in the form of bent extrusions (shadow arrows) accompanied by intrusions.

interface dislocation is parallel to the surface, the pile-up of these dislocations acts against the grain boundary. Then the locally increased stresses cause decohesion of the GB under the external tensile loading. However, it was found that the impingement of PSBs with the favourably oriented Burgers vector forms PSMs at GB and cause the plastic incompatibility along the grain boundary. Extrusions grow during cycling and exert normal stress on the neighbour grain so high that extrusions are highly bent (see Fig. 4.1.4). Several parallel extrusions along the GB continuously push away the neighbouring grain. Moreover, if we consider the formation of the PSM in the form of the extrusion and intrusion pair as proposed by Polák [30] the intrusions are present at GB as well. The simultaneous growth of extrusions pushing away the GB and presence of the intrusions at GB lead to the grain boundary cracking. The intrusions act as the local discontinuities at grain boundary leading to partial decohesion and weakening of the GB.

Only a few fatigue cracks initiated at GBs were observed. The initiated grain boundary crack grows later along the slip planes inclined at about 45 degrees to the loading direction (see Fig. 4.1.4). The detail in Fig. 4.1.4 shows the significant role of the PSBs having the Burgers vector almost parallel to the surface (favourably oriented) and producing the fatigue induced relief at GB. The slip systems playing a role in the GB cracking are highly misoriented so that the PSM in one grain cannot continue in the neighbouring grain thus being stopped at GB. The GB is oriented to be perpendicular to the tensile loading where the GB is subjected to opening Mode I crack growth [39].

The cracking mechanism of the GBs due to the impingement of the PSBs at a GB was proposed by Christ et al. [40]. The mechanism is based on the emerging of the PSBs at the surface and formation of the fatigue induced relief according to the EGM model [29]. They consider the role of the interface edge dislocations located at the interface between PSB and matrix. In a grain where the component of Burgers vector of



#### 4.1.2 Crack growth of natural cracks

The natural short fatigue cracks propagate in two stages of the crack growth. The first period is the crack initiation and early crack growth along PSM/PSB denoted as Stage I and the second is the crack growth approximately perpendicular to the loading axis denoted as Stage II [41]. Fatigue crack

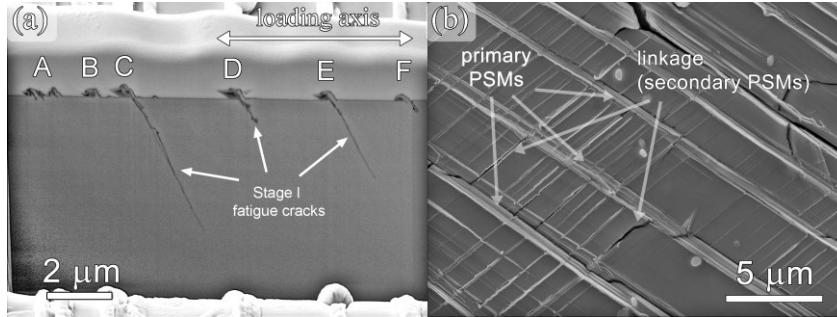


Figure 4.1.5: FIB section of a grain showing multiple crack initiations inside the grain and early growth in crystallographic direction (a); linking of cracks, which initiated in parallel PSMs by secondary cracks after further cycling (b).

initiation plays an important role in the fatigue life of the cyclically strained bodies since without the crack initiation there is no crack growth and no fracture. Nevertheless, in the low cycle fatigue domain the period of the crack initiation is usually not life determining. Early and easy crack initiation can however shorten the fatigue life.

Stage I fatigue crack growth

follows, similar to the 316L [4] steel, the highest shear stress planes oriented approximately 45 degrees in relation to the applied load (see Fig. 4.1.5). As expected Stage I crack growth has a crystallographic character affected by the structure of the material (grain size, grain disorientation...) and by the fatigue

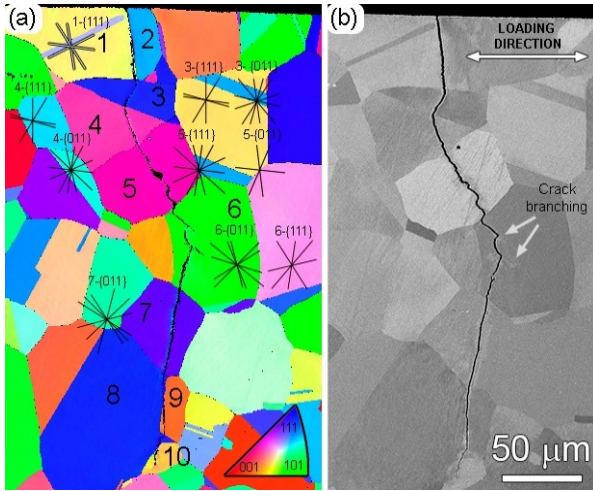


Figure 4.1.6: Crack path in the bulk of the material. The sample was subjected to loading the  $\varepsilon_a = 0.25\%$ . Loading direction is horizontal. (a) EBSD analysis showing the grains orientation with individual  $\{111\}$  and  $\{011\}$  slip plane traces. The corresponding IPF map is included. (b) ECCI

induced dislocation microstructure (see Chapter 4.1.1a) leading to the formation of the surface relief. The high number of PSMs on the surface and subsequently the more frequent crack initiation was found in the materials frequent crack initiation was found in the materials with high nitrogen content [42] what is in agreement with our observations. The high activity of the slip systems also increases the initiation probability along the GBs and TBs as shown earlier. The Stage I crack (initiated along the PSM/PSB) grows under the shear loading during the tensile part of the cycle (see Fig. 4.1.5). Nevertheless, it has been observed, that the Stage I crack growth often does not exceed the length of the grain size. More commonly, the crack growing in Stage I deflects from its original crack path and continues to propagate perpendicular to the loading direction which is denoted as the Stage II crack growth (see Fig. 4.1.6). The early growth of the Stage I crack is characterized by the mutual interlinking of small semi-elliptical

shallow cracks developed along the PSMs as observed in 316L steel [4] (see Fig. 4.1.5b). Later, when the microstructurally small crack are large enough the parallel cracks within one grain link together typically along the  $\{111\}$  slip planes. Those are frequently associated with the emerging slip markings on the grain surface (see Fig. 4.2.1b). The surface length of the Stage I cracks is of the structural unit length. Similar observations were performed by Lindstedt [42] and Zhixue [43] on 316 austenitic steel. The zig-zag path of the Stage I cracks leads to the decrease of the crack growth rates as a result of the

roughness-induced crack closure. On the other hand, the early crack linkage within one grain might increase the crack growth rate of the Stage I crack.

Stage II short cracks follow preferentially the low indexed slip planes (e.g.  $\{011\}$  or  $\{001\}$ ) as shown in Fig. 4.1.6. The higher is the applied strain amplitudes, the higher fraction of crack growth belongs to the low indexed slip planes. The fracture surface is characteristic in striations implying the extend of the crack front under the effect of two active slip systems. Since several Stage II short cracks has initiated at the surface their further growth is influenced by mutual coalescence. It is in agreement with the observations performed on the cycled 316 stainless steel [42-44] that the fraction of the surface cracks increases till the half of the lifetime. Later the fraction of the surface cracks decreases. This implies that initiated cracks link together and the linking of the cracks contributes to the growth of the cracks. In high strain amplitude loading usually one crack becomes dominant crack and plastic strain is concentrated to its crack tip plastic zone. Moreover, the stress-shielding effect coming from the stress-free crack surfaces of the dominant crack causes the shielding of other cracks and only dominant crack propagates.

#### *4.1.3. Crack growth kinetics of short natural cracks and fatigue life*

Natural cracks initiate predominantly in PSMs as the shallow surface cracks. Usually, the crack is initiated in 1, 2, or up to 3 neighboring grains simultaneously. The depth of the initiated crack varies considerably but generally is lower than the half of the surface length. As the surface crack length increases, the shape of the crack gets closer to the shape of a semicircle. Blochwitz and Richter [16] evaluated the ratio of the projected crack depth to the projected surface crack length approximately to 0.44. Because the deviation from the semicircle is low, we have characterized the size of the crack by the half of the surface crack length projected to the plane perpendicular to the loading axis. It is approximately equal to the radius  $a$  of a semicircle projected to this plane. Figure 4.1.7 shows the semilogarithmic plot of the crack length  $a$  of the longest cracks vs the number of cycles in specimens cycled with strain amplitudes in the range from  $2.5 \times 10^{-3}$  to  $7 \times 10^{-3}$ .

The growth of the individual cracks at the beginning of the cycling for all strain amplitudes is influenced by the microstructure of the material (i.e. grain orientation). The high angle grain boundaries represent the effective barriers for the further crack growth [45]. As the crack length increases the increment of the crack rate becomes more stable. Though several cracks grow simultaneously at approximately the same rate (see Fig. 4.1.7), different physical crack can become instantaneously the longest crack in the notch. Based on the study by Polák et al. [46] these two facts allow approximating the growth of all cracks growing under the cycling with constant strain amplitude by one representative crack. This crack is called the equivalent crack. Since we cannot follow the growth of the crack in the bulk in the case of linkage of two cracks we can only omit the points which do not correspond to the growth of the cracks having the “semi-circular” shape. If the crack length suddenly increased and stopped its further growth at the surface for some time it indicates the cracks linkage and the growth of the interlinked crack in the bulk. Therefore, only the points before and after the full crack coalescence are considered as growth of the equivalent crack.

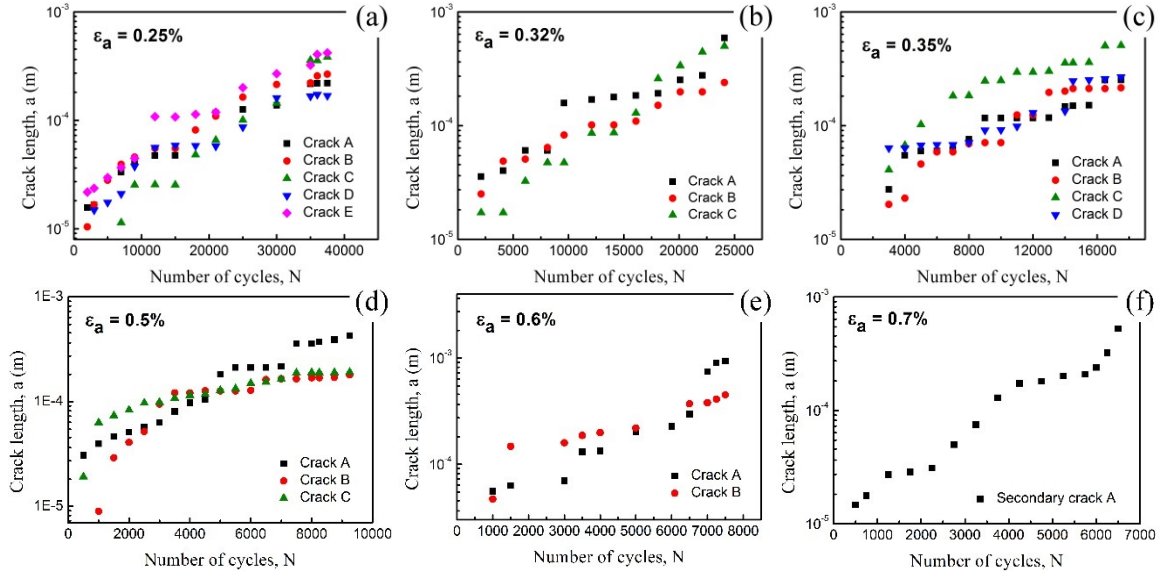


Figure 4.1.7: Semi-logarithmic plot of crack length  $a$  vs number of cycles  $N$  for different total strain amplitudes  $\epsilon_a$ . (a)  $\epsilon_a = 0.25\%$ , (b)  $0.32\%$ , (c)  $0.35\%$ , (d)  $0.5\%$ , (e)  $0.6\%$ , (f)  $0.7\%$ .

Short fatigue crack growth rates can be described using fracture mechanics approaches. The stress intensity factor is often chosen as the parameter characterizing the propagation of cracks the crack growth rate of the equivalent crack is plotted versus stress intensity amplitude  $K_a$ . It was shown in Sanicro 25 that with increasing applied strain amplitude propagation rates increases [47]. According to Ritchie [48] the loading with strain amplitude resulting in appreciable plastic strain amplitude enhances the cyclic plastic zone ahead of the crack front. Since the stress intensity factor is applicable for small scale yielding when the plastic zone is much smaller than the crack length the description of the stress field around the crack tip based on the stress intensity factor is not appropriate. This is called the physically short crack effect [48].

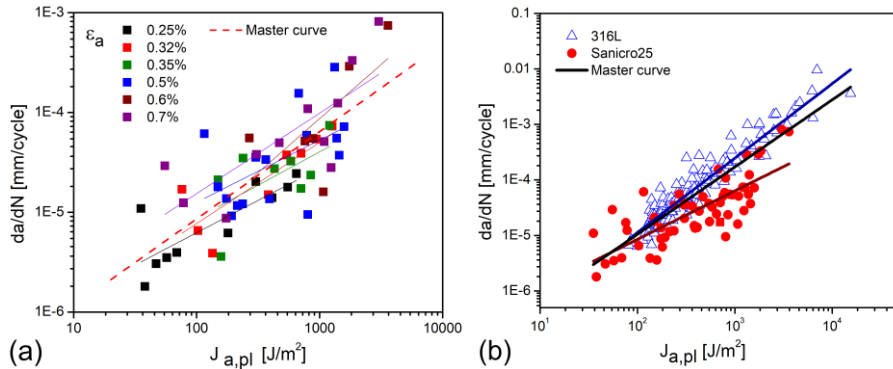


Figure 4.1.8: a) Short crack growth rate vs. plastic part of  $J$ -integral for Sanicro 25 steel for individual equivalent cracks growing under cycling with  $\epsilon_a$  in the range from  $0.25\%$  to  $0.7\%$ . b) Short crack growth rate vs. plastic part of  $J$ -integral for Sanicro 25 steel and 316L steel.

Mode I. It was reported earlier [50] that during the low cycle fatigue the fraction of the plastic part of  $J$ -integral increases with increasing applied total strain amplitude. It was concluded that the plastic component of  $J$ -integral plays the main role in the short crack growth.

Therefore, the parameter describing the intensity of elastic-plastic stress field ahead of the crack front has to be used as proposed by Rice [49]. The crack propagation rate can be characterized by  $J$ -integral.  $J$ -integral is composed of two, the elastic and plastic component, and can be estimated for loading



Nevertheless, the plot of crack growth rates of equivalent cracks vs. the plastic component of  $J$ -integral (see Fig. 4.1.8a) still shows appreciable scatter. The dependence on the applied strain amplitude remains. The high scatter in the values of crack growth rates may be caused by the mutual linkage of the initiated short cracks. During the coalescence of two cracks the plastic zone ahead of the crack front varies and this can also affect the crack growth rate. Nevertheless, even in the case of scatter the dependence of the crack growth rate on the  $J_{ap}$  can be extrapolated by the Master curve (Eq. 4.1.1) with the parameters  $C_{Jp} = 1.522 \times 10^{-7}$  and  $m_{Jp} = 0.874$  characterizing the crack propagation in Sanicro 25.

$$\frac{da}{dN} = C_{Jp} \left( \frac{J_{a,pl}}{J_{a,pl,0}} \right)^{m_{Jp}} \quad (4.1.1)$$

$J_{a,pl,0}$  is a constant equal to 1 J/m<sup>2</sup> in order to simplify the units of  $C_{Jp}$  and  $m_{Jp}$  constants.

The Master curve of Sanicro 25 is compared with the Master curve derived for 316L [50] steel in Fig. 4.1.8b. It shows that the 316L steel exhibits higher crack growth rates for the same plastic component of the  $J$ -integral when compared to those of the Sanicro25 steel. The parameters of the Eq. 4.1.1 for 316L steel are  $C_{Jp} = 2.341 \times 10^{-8}$  and  $m_{Jp} = 1.342$ . Nevertheless,

the Master curve describing the crack grow rates of both materials is derived as well and the parameters are as follows  $C_{Jp} = 3.970 \times 10^{-8}$  and  $m_{Jp} = 1.212$ .

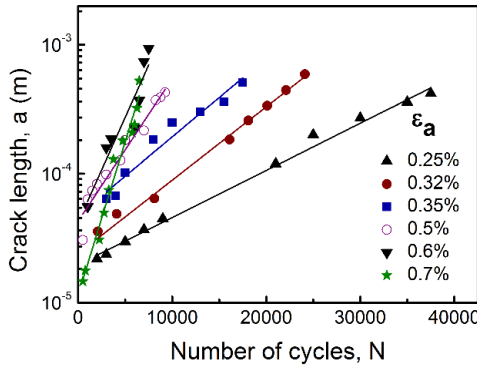


Figure 4.1.9: Length of equivalent semi-circular cracks vs. number of cycles in cycling with constant total strain amplitude in the range of  $(2.5-7.0) \times 10^{-3}$ .

The difference can be due to the cyclic plastic deformation in the case of Sanicro 25 steel is localized into the narrow PSBs (see Chapter 4.1.1a) leading to the smaller plastic zone ahead of the crack tip than in the 316L steel. Therefore, the crack tip blunting may be smaller than that in the case of 316L steel leading to the smaller crack increment in one cycle. The effective value of the  $K_a$  can be also decreased due to the high planar character of dislocation slip.

Alternative approach to the fracture mechanics on the characterization of the short crack growth is crack growth law presented by Polák [51]. Figure 4.1.9 shows the semi-logarithmic plots of the lengths of all equivalent cracks vs. the number of cycles. The data show a good linear dependence in the semi-logarithmic plot. The data were thus fitted by the exponential law corresponding to

$$a = a_i \exp(k_g N) \quad (4.1.2)$$

where  $a$  is the crack length,  $a_i$  is the crack length extrapolated back to zero number of cycles and  $k_g$  is crack growth coefficient and  $N$  is the number of cycles. Both parameters  $a_i$  and  $k_g$  were evaluated using least-square regression analysis procedure. The extrapolated initial crack length does not show a systematic dependence on the strain amplitude. The average value was 27 μm, which is approximately the half of the average grain size of the material. In contrast to that, the crack growth coefficient increases systematically with the increasing applied strain amplitude. Since the fatigue life in the regime of low cycle fatigue is dependent on the plastic strain amplitude as observed by Manson and Coffin [52; 53] we shall correlate  $k_g$  coefficient with the plastic strain amplitude evaluated in the notch as follows

$$k_g = k_{g0} \varepsilon_{ap}^d \quad (4.1.3)$$

where  $k_{g0}$  is constant and  $d$  is crack growth exponent. The plastic strain amplitude increased by the notch effect plays an important role in crack growth. Then the parameters representing the crack growth law derived for Sanicro 25 steel in Eq. 4.1.3 are as follows:  $k_{g0} = 0.544$  and  $d = 1.393$ .

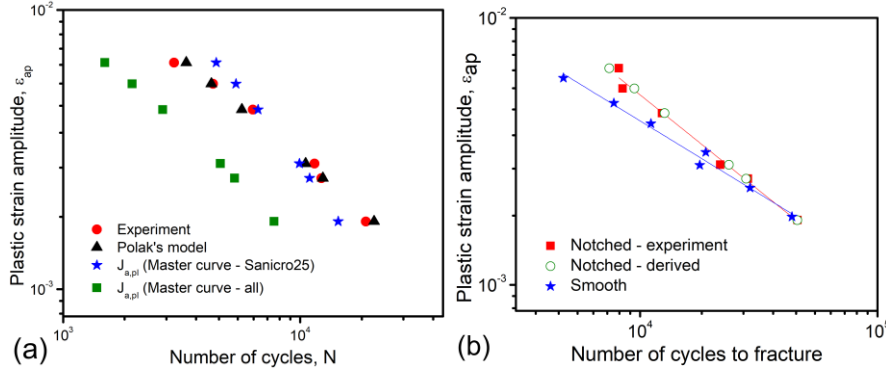


Figure 4.1.10: a) Dependency of the plastic strain amplitude  $\epsilon_{ap}$  and the number of cycles  $N$ , which corresponds to the number of cycles spend on the crack extend from 0.1 mm to 0.5 mm in the Sanicro25 steel. b) Manson-Coffin fatigue life curves of Sanicro25 steel (smooth [14] and notched specimens) compared with the Polák's crack growth law.

The number of cycles needed to extend the crack length from the initial crack length  $a_0$  to the final crack length  $a_f$  can be estimated integrating equations 4.1.1, 4.1.2. To compare the estimated number of cycles using crack growth law or using  $J_{a,pl}$  with the experimental ones, the interval of the physically short crack length 0.1 - 0.5 mm, in which the crack lengths

were measured, was chosen.

Figure 4.1.10a shows the measured and derived number of cycles needed to extent the crack length from 0.1 mm to 0.5 mm. The number of cycles calculated using parameters  $k_{g0}$  and  $d$  of the Polák's model give very good agreement with the experimental data. Contrary to that the number of cycles calculated analytically using  $J_{a,pl}$  with parameters derived for the Sanicro 25 steel shows higher slope of the linear fit. The highest deviation from the experimental data shows plot using the Master curve derived for both steels 316L and Sanicro 25. The reason is that the Master curve in Fig. 4.1.8b is well above the data of Sanicro 25. It indicates that one Master curve cannot characterize several materials with different material properties.

Provided that the initiation and growth of all fatigue cracks can be substituted by the growth of an equivalent crack from the initial crack length,  $a_i$ , up to final crack length,  $a_f$ , which follows the crack growth law (see Eq. 4.1.2) and the crack growth coefficient,  $k_g$ , depends on the plastic strain amplitude according to the Eq. 4.1.3 the crack growth law can be integrated and fatigue life is obtained using parameters of the crack growth law. Additionally, it was shown earlier by Polák [51] and Polák and Zezulka [54] that the parameters of the short crack growth law and the parameters of the Manson-Coffin law are related as follows:

$$d = -\frac{1}{c} \quad k_{g0} = 2(\epsilon_f')^{1/c} \ln\left(\frac{a_f}{a_i}\right) \quad (4.1.4)$$

The parameters of the short crack growth law can be thus evaluated from the parameters  $c$  and  $\epsilon_f'$  determined from the Manson-Coffin curve (Eq. 4.1.4) provided the ratio of the final to the initial crack length is estimated. Similar to that, the parameters of the Manson-Coffin law can be inversely evaluated using the parameters of the crack growth law  $k_{g0}$  and  $d$  (see Eq. 4.1.4.).

The fatigue life curves of previously measured smooth cylindrical specimens [14] and currently measured notched cylindrical specimens are compared in Fig. 4.1.10b. Along with the experimentally measured data, the derived fatigue life curve estimated using the parameters of the Manson-Coffin law evaluated from the crack growth law parameters of notched specimens (using the Eq. 4.1.4) is plotted

as well. The number of cycles to fracture was estimated by integrating derived Manson-Coffin law. Since the parameter  $\varepsilon_f'$  depends on the ratio of the initial crack length and final crack length, the initial crack length for Sanicro 25 steel was put equal to half of the grain size  $27\text{ }\mu\text{m}$  and  $1\text{ mm}$  was considered as the final crack length.

Both derived and experimentally measured Manson-Coffin laws of notched specimens lie very close (see Fig. 4.1.10b). It indicates that the crack growth under the cyclic plastic strain determines the fatigue life of the specimen under low cycle fatigue conditions. Then the parameters of the short crack growth law can be reasonably well used to evaluate the parameters of the Manson-Coffin law and to determine the residual fatigue life of the sample (see Tab. 4.1.1). The small difference between the Manson-Coffin law measured on smooth specimens and the derived curve for notched specimens can be explained by the effect of the different surface preparation and also the effect of plastic strain gradient in the notch. The smooth samples were finally ground while the surface of notched specimen was electrolytically polished. The gradient of plastic strain can have different effect on crack growth rates for small and high plastic strain amplitudes.

Samples	Manson-Coffin curve				Crack growth law			
	$\varepsilon_f'$		$c$		$k_{g0}$		$d$	
	exp.	der.	exp.	der.	exp.	der.	exp.	der.
Smooth	<b>7.22</b>		<b>-0.718</b>			0.754		1.393
Notched		6.404		-0.718	<b>0.544</b>		<b>1.393</b>	

Table 4.1.1: Parameters of the **experimentally measured** and calculated crack growth law and Manson-Coffin law for both smooth and notched specimens.

## 4.2. Fatigue at temperature of 700°C

### 4.2.1. Grain boundary oxidation and crack initiation

High temperature fatigue damage mechanisms in austenitic stainless steels differ appreciably from that at room temperature [6]. Room temperature cyclic straining of Sanicro 25 is characterized by the strong localization of the cyclic plastic strain into the narrow persistent slip bands [55] and the crack initiation starting from the PSMs, especially from the tip of the intrusions (see Fig. 4.1.2). Contrary to that, the high temperature enhances temperature activated cross slip of dislocations and thus the localization of the cyclic plastic strain is more difficult as observed previously in 316L steel [56]. Furthermore, in the case of Sanicro 25 steel, the motion of dislocations is limited by their pinning by the Nb(CN) nanoprecipitates, which nucleated during the fatigue [57]. Therefore, the localization of the cyclic plastic strain into the PSBs is very difficult. Due to that, the appearance of the extrusions along the PSBs within the grains at the surface is very sporadic and no cracks were observed to initiate from extrusions.

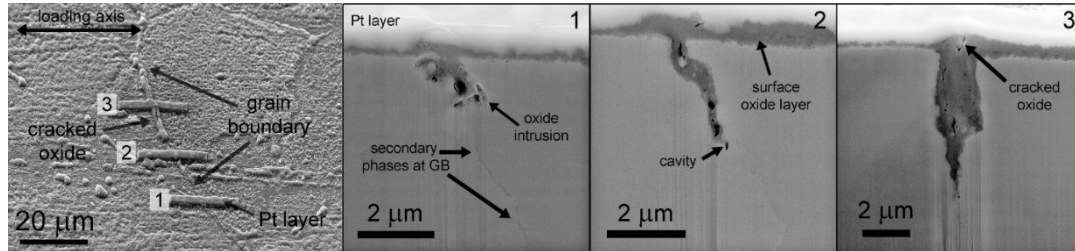
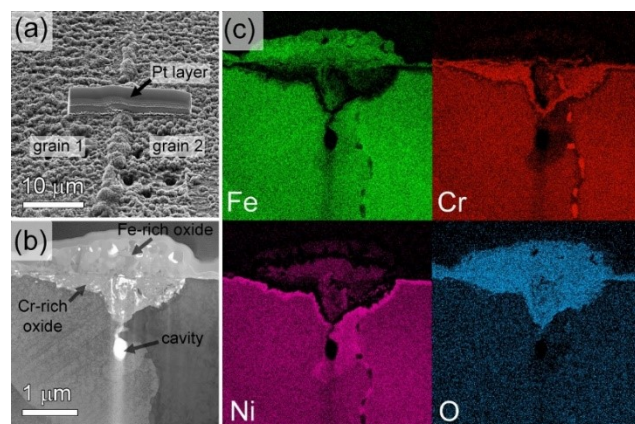


Figure 4.2.1: Cracked oxide extrusion at the grain boundary subjected to the SEM/FIB study. The FIB cuts denoted by numbers are shown in the details.

The oxidized GBs were found to be the primary crack nucleation site. It is due to the easier penetration of the oxygen into the material by means of the motion of vacancies under the external loading or by



*Figure 4.2.2: (a) SEM micrograph of the surface with the oxide nodules grown at the GB. Deposited platinum layer marks the position of the TEM lamella extraction. (b) BF STEM image of extracted TEM lamella. Oxide intrusion grew along the GB. Cavity was found at the tip of the oxide intrusion. (c) STEM-EDS map analysis of the oxide and surrounding matrix. Oxide layer is formed of the outer layer enriched in Fe and inner layer enriched in Cr. Layer heavily enriched in Ni is clearly distinctive in the austenitic matrix close to the oxides. Notably Ni-enriched area is observed also below the oxide intrusion (around the cavity).*

depleted in Cr and Fe. The results are in a good agreement with the experimental work of Rothman et al. [59], who measured that the diffusion rate of Ni in the Fe-Cr-Ni based alloy system is notably lower when compared to that of Cr and Fe. Considering the fact that the diffusion rate of Ni is several times lower than that of Cr and Fe [59], it is natural that vacancies bound to Fe and Cr atoms flowing to the interface condense forming a cavity.

Since, the grain boundaries are the preferential sites for the oxidation, the crack nucleation appears as the rupturing of the brittle GB-oxide under tensile load. Therefore, preferentially GBs oriented approximately perpendicular to the loading axis have been cracked. Moreover, the resistance of the GB-oxides to the rupturing is decreased by the presence of the cavities acting as the stress concentrators under the repeated external loading in the high temperature low cycle fatigue. After the rupture of the GB-oxide the freshly exposed metal is subjected to further oxidation.

Moreover, it is worthy to note that despite the loading rate at high temperatures in LCF conditions can be considered as relatively low, no damage mechanisms as diffusion induced creep damage was observed. It is known that the creep damage in the form of cavitation at the interfaces accelerates the crack growth rate leading to short fatigue life. In the case of Sanicro 25 steel, the damage of the material in the form of cavitation was reported only in the presence of dwell period in a cycle [60].

high temperature activation of diffusion preferentially in HAGBs (see Fig. 4.2.1). Moreover, according to work of Trillo and Murr [58], an incoherent grain boundary might present the primary nucleation site for the Cr-rich  $M_{23}C_6$  carbide precipitation at high temperatures. As a result, heavily Cr-depleted zones are formed at the GBs [58] as well as at the carbide/matrix interfaces as shown in Fig. 4.2.2 facilitating the oxidation of the GB.

The early GB oxidation is characterized by the growth of the internal oxide intrusion in the form of the Cr-rich layer. Such an oxide layer should create the protective layer against further penetration of the oxygen into the material and diffusion of the metallic elements to the surface. Nevertheless, as is shown in Fig. 4.2.2c oxide layer consists of outer scales enriched in Fe further from the matrix and Cr-rich scales close to the oxide/matrix interface. The Cr-rich layer is found to be porous which probably promotes further oxidation of the material. Below these oxide layers, thick oxidation-affected zone is formed in the matrix. This zone is heavily enriched in Ni and



#### 4.2.2. Crack growth under environmental conditions

Surface cracks and cracks growing in the bulk were inspected and the fractions of the crack path corresponding to trans- and intergranular growth were evaluated (see Fig. 4.2.3). Since GB oxidation causes multiple crack initiation due to the cracked oxides later leading to the crack coalescence the

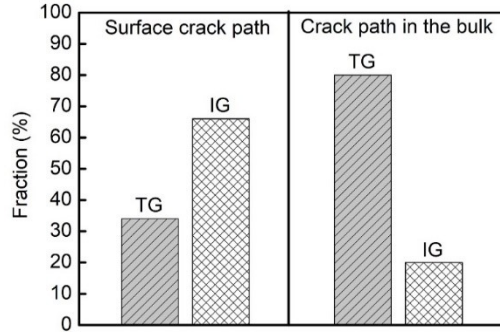


Figure 4.2.3: Fractions of the crack paths corresponding to the transgranular (TG) and intergranular (IG) growth at the surface and in the bulk of the material.

intergranular growth on the surface prevails. The average fractions of the total length of the surface cracks growing intergranularly and transgranularly were about 66% and 34%, respectively. Contrary to that the average fraction of the total length of the cracks in the bulk of the material growing trans- and intergranularly was about 80% and 20%, respectively. It is apparent that the multiple crack initiation along the oxidized GBs significantly affects the growth behavior of the cracks close to the surface. Cracks grow preferentially in the intergranular manner as shown in the statistical analysis in Fig. 4.2.3. Later, with further cycling, initiated cracks link together. As a result, the crack growth rates of the surface cracks rapidly increase.

The growth paths of the surface cracks are in contrast with the crack paths in the bulk of the material, where the transgranular character of the crack growth prevails (see 4.2.3). The crack grows under the action of the cyclic plastic deformation ahead of the crack tip similarly as in the case of the crack growth at room temperature. This is in accordance with the appearance of the plastic zone localized along the crack path and in front of the crack tip. The observations of the transgranular crack growth are in a good agreement with the works of Pavinich et al. [7] and Yamaguchi et al. [8]. Pavinich et al. [7] studied the effect of the grain size, temperature, and the strain rate on the character of the crack path in polycrystalline copper containing a silica particles. They found that the transgranular crack path notably

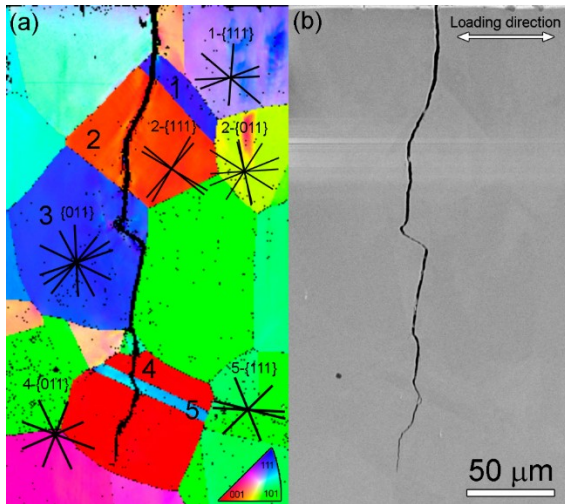


Figure 4.2.4: EBSD analysis of the crack path in the bulk of the material. The corresponding slip plane traces are included for each of the grains. (a) EBSD map. (b) Secondary electron image.

predominates over the intergranular path even at high temperatures. This tendency is stronger at higher strain rates. Similar observations were presented by Yamaguchi et al. [8], who studied the effect of the strain wave shape on the high temperature fatigue behavior of a 316 type steel at 600 °C and 700 °C. Fractographic observations revealed that in the testing with the slow triangular wave shape the fracture surface was of the intergranular character, while in the fast triangular wave shape tests fracture surface was of the transgranular character and the fatigue life was longer.

The role of the plastic deformation in the crack growth is notable also from the Fig. 4.2.4. The cracks propagate approximately perpendicular to the loading axis preferentially following the low indexed crystallographic planes of type  $\{011\}$  and  $\{001\}$ . As shown in Fig. 4.2.5 the crack propagates under the coactive action of several slip systems of type  $\{111\}\langle 011\rangle$  as was earlier proposed by Neumann [61] for the crack propagation at room temperature.

The plastic zone ahead of the crack tip can be recognized due to the high lattice distortion and subsequently the loss of the diffraction contrast. The growth of the crack under the cyclic plastic

deformation along with the oxidation and rupturing of the brittle oxides can increase the crack growth rate and decrease the fatigue life compared to the cycling at a room temperature.

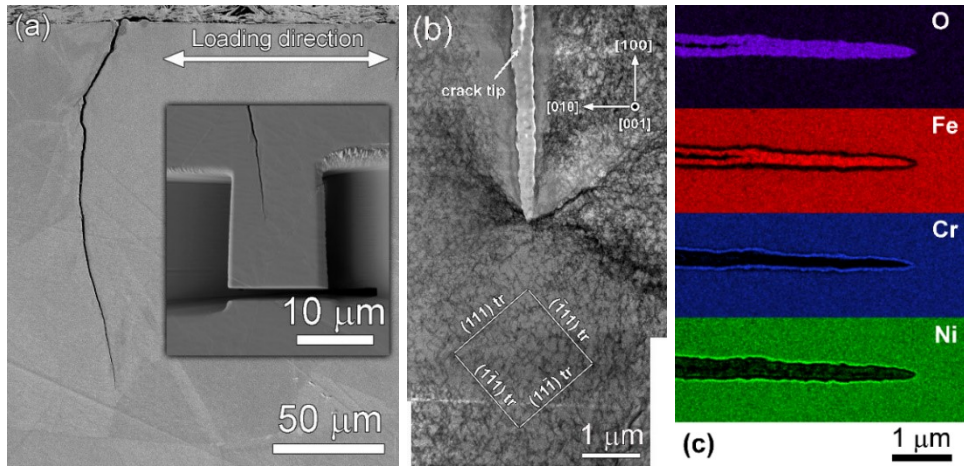


Figure 4.2.5: a) SE micrograph of the crack. Inset shows the position of the lamella. b) BF-STEM of the oxidized crack tip with the surrounding dislocation microstructure. c) EDS maps showing the chemical composition of the oxide at the crack tip and surrounding matrix.

## 5. CONCLUSIONS

The experimental study of low cycle fatigue damage of advanced alloy based on Fe-Ni-Cr matrix tested both at room temperature and at a temperature of 700°C led to the following conclusions:

- The high planar character of the dislocation slip in the material leads to the cyclic plastic strain localization into the narrow persistent slip bands of about 200 nm in thickness during the cycling at room temperature. Owing to the absence of the dislocations from secondary slip systems within the PSBs, the PSBs can be clearly distinguished in the matrix.
- Dislocation structure of well-developed persistent slip bands producing persistent slip markings does not need to be ladder-like. Nevertheless, it must accommodate the local intensive cyclic slip. Dislocation-rich and dislocation-poor regions are present in the persistent slip bands. The complicated shape of the persistent slip markings consisting of extrusions and intrusions is compatible with the internal dislocation structure of PSBs.
- Three specific types of sites of crack initiation leading to the growth of the major cracks were found on the samples cyclically strained at room temperature: (i) along the fatigue induced surface relief in the form of persistent slip markings, (ii) twin boundaries and (iii) grain boundaries. Although the role of TBs and GBs was observed to increase with the increase of the applied total strain amplitude the role of PSMs prevail in all strain amplitudes.
- The cracks were observed to start along the PSMs from the tip of the intrusions or intrusion-like defects. The intrusion can be easily distinguished from the stage I crack since its vortex angle is of about 10 degrees. The vortex angle of the crack is equal to zero degree.

- In the case of high angle GBs cracking one of the primary slip systems of the grains must be parallel with the surface. The PSMs emerging in the GB oriented perpendicular to the surface and to the loading direction cause the local incompatibilities leading to final decohesion of the GB under the tensile loading.
- Cracks initiated in PSMs grow predominantly along the  $\{111\}$  slip planes due to high plastic strain localization in PSBs. Grain boundaries, secondary phases etc. locally slow down the crack growth rate of microstructurally short cracks. The mutual coalescence of the cracks increases the surface crack length and thus contributes to crack growth acceleration of natural short cracks. Then, the equivalent crack length can reasonably well describe the damage evolution in cyclic straining with constant strain amplitudes.
- The crack growth rate was found to be proportional to the crack length. It corresponds to the exponential increase of the crack length. The crack growth coefficient characterizes the dependence of the growth rate on the applied plastic strain amplitude. The power law dependence of the crack growth coefficient corresponds to the Manson-Coffin law. The parameters of the crack growth law can be thus derived from the parameters of the Manson-Coffin law. The correlation of the crack growth rate with the plastic part to the  $J$ -integral gives a high scatter.
- The crack initiation during the cyclic loading at elevated temperature was found to be along the oxidized GBs. High interfacial energy and the presence of numerous lattice defects such as vacancy-type defects at the grain boundaries significantly facilitate oxygen diffusion and lead to notably enhanced oxidation. Cavities are formed at the tip of the oxide intrusion presumably as a result of different diffusion rates of elements and the Kirkendall effect.
- The cracking of the oxides at the grain boundaries is the main cause of very early fatigue crack initiation in these sites. Highly porous brittle oxides located at the grain boundaries perpendicular to the loading axis fracture as a result of external tensile stress. Fracture of oxides facilitates further diffusion of oxygen from the air to the crack tip. The growth of the oxide intrusion and also of the surface crack proceeds.
- There is a difference between the mechanisms of fatigue crack propagation on the surface and in the bulk of the material. Rapid increase of crack density on the surface as a result of the fracture of oxidized grain boundaries leads to their linkage. Long surface cracks have high driving force for the growth in the bulk and both intergranular as well as transgranular crack paths are observed. Transgranular path is due to the localization of plastic deformation and formation of the cyclic plastic zone ahead of the crack tip. Rapid crack initiation due to the oxide cracking and rapid growth of the long surface cracks leads to substantial decrease of the fatigue life in comparison with the room temperature cyclic loading.

## 6. REFERENCES

- [1] CHAI, G. C., T. SAND, J. HERNBLOM, U. FORSBERG AND T. PELTOLA. Development of Advanced Heat Resistant Materials for IGCC and AISC Power Plants. In *Energy Materials 2014*, Springer, Cham, 2014, 227-234. DOI: 10.1007/978-3-319-48765-6\_25
- [2] POLÁK, J. *Cyclic plasticity and low cycle fatigue life of metals*. Edition ed. Amsterdam: Elsevier, 1991. ISBN 978-80-200-0008-8.
- [3] EWING, J. A. AND J. C. W. HUMFREY. The fracture of metals under repeated alternations of stress. *Philosophical Transactions of the Royal Society A*, 1903, **200**, 241-250. DOI: 10.1098/rsta.1903.0006
- [4] MAN, J., P. KLAPETEK, O. MAN, A. WEIDNER, K. OBRTLÍK AND J. POLÁK. Extrusions and intrusions in fatigued metals. Part 2. AFM and EBSD study of the early growth of extrusions and intrusions in 316L steel fatigued at room temperature. *Philosophical Magazine*, 2009, **89**(16), 1337-1372. DOI: 10.1080/14786430902917624
- [5] MAN, J., K. OBRTLÍK AND J. POLÁK. Extrusions and intrusions in fatigued metals. Part 1. State of the art and history. *Philosophical Magazine*, 2009, **89**(16), 1295-1336. DOI: 10.1080/14786430902917616
- [6] PINEAU, A. AND S. D. ANTOLOVICH. High temperature fatigue: behaviour of three typical classes of structural materials. *Materials at High Temperatures*, 2015, **32**(3), 298-317. DOI: 10.1179/0960340914Z.000000000072
- [7] PAVINICH, W. AND R. RAJ. Fracture at elevated temperature. *Metallurgical Transactions A*, 1977, **8**(12), 1917-1933. DOI: 10.1007/BF02646566
- [8] YAMAGUCHI, K. AND K. KANAZAWA. Effect of Strain Wave Shape on High-Temperature Fatigue Life of a Type-316 Steel and Application of the Strain Range Partitioning Method. *Metallurgical Transactions A*, 1980, **11**(12), 2019-2027. DOI: 10.1007/BF02655121
- [9] COFFIN, L. F. The effect of frequency on the cyclic strain and fatigue behavior of cast René at 1600° F. *Metallurgical Transactions A*, 1974, **5**(5), 1053-1060. DOI: 10.1007/BF02644317
- [10] MCMAHON, C. J. AND L. F. COFFIN. Mechanisms of damage and fracture in high-temperature, low-cycle fatigue of a cast nickel-based superalloy. *Metallurgical Transactions*, 1970, **1**(12), 3443-3450. DOI: 10.1007/BF03037877
- [11] CHAI, G. AND U. FORSBERG. Sanicro 25: an advanced high-strength, heat resistant austenitic stainless steel. In A. DIGIANFRANCESCO ed. *Materials for Ultra-Supercritical and Advanced Ultra-Supercritical Power Plants*. Amsterdam: Elsevier, 2017, p. 391-421. DOI: 10.1016/B978-0-08-100552-1.00012-9
- [12] SOURMAIL, T. Precipitation in creep resistant austenitic stainless steels. *Materials Science and Technology*, 2001, **17**(1), 1-14. DOI: 10.1179/026708301101508972
- [13] KORZHAVYI, P. A. AND R. SANDSTROM. First-principles evaluation of the effect of alloying elements on the lattice parameter of a 23Cr25NiWCuCo austenitic stainless steel to model solid solution hardening contribution to the creep strength. *Materials Science and Engineering A*, 2015, **626**, 213-219. DOI: 10.1016/j.msea.2014.12.057
- [14] POLÁK, J., R. PETRÁŠ, M. HECZKO, I. KUBĚNA, T. KRUMML AND G. C. CHAI. Low cycle fatigue behavior of Sanicro25 steel at room and at elevated temperature. *Materials Science and Engineering a-Structural Materials Properties Microstructure and Processing*, Oct 6 2014, 615, 175-182.



- [15] OBRTLÍK, K. AND J. POLÁK. Fatigue Growth of Surface Cracks in the Elastic-Plastic Region. *Fatigue and Fracture of Engineering Materials and Structures*, 1985, **8**(1), 23-31. DOI: 10.1111/j.1460-2695.1985.tb00417.x
- [16] BLOCHWITZ, C. AND R. RICHTER. Plastic strain amplitude dependent surface path of microstructurally short fatigue cracks in face-centred cubic metals. *Materials Science and Engineering A*, 1999, **267**(1), 120-129. DOI: 10.1016/S0921-5093(99)00060-X
- [17] LUKÁŠ, P., M. KLESNIL AND J. KREJČI. Dislocations and Persistent Slip Bands in Copper Single Crystals Fatigued at Low Stress Amplitude. *Physica Status Solidi B*, 1968, **27**(2), 545-558. DOI: 10.1002/pssb.19680270212
- [18] LAIRD, C., P. CHARLEY AND H. MUGHRABI. Low-Energy Dislocation-Structures Produced by Cyclic Deformation. *Materials Science and Engineering*, 1986, **81**, 433-450. DOI: 10.1016/0025-5416(86)90281-8
- [19] MUGHRABI, H., F. ACKERMANN AND K. HERZ. Persistent Slipbands in Fatigued Face-Centered and Body-Centered Cubic Metals. In J. FONG. *Fatigue Mechanisms*. West Conshohocken: ASTM International, 1979, p. 69-105. DOI: 10.1520/STP35885S
- [20] POLÁK, J., S. DEGALLAIX AND G. DEGALLAIX. The Role of Cyclic Slip Localization in Fatigue Damage of Materials. *Journal De Physique IV France*, 1993, **3**(C7), 679-684. DOI: 10.1051/jp4:19937107
- [21] WEIDNER, A., R. BEYER, C. BLOCHWITZ, C. HOLSTE, A. SCHWAB AND W. TIRSCHLER. Slip activity of persistent slip bands in polycrystalline nickel. *Materials Science and Engineering A*, 2006, **435-436**, 540-546. DOI: 10.1016/j.msea.2006.07.039
- [22] HUNSCH, A. AND P. NEUMANN. Quantitative Measurement of Persistent Slip Band Profiles and Crack Initiation. *Acta Metallurgica*, 1986, **34**(2), 207-217. DOI: 10.1016/0001-6160(86)90192-6
- [23] GERLAND, M., J. MENDEZ, P. VIOLAN AND B. A. SAADI. Evolution of Dislocation-Structures and Cyclic Behavior of a 316L-type Austenitic Stainless-Steel Cycled in Vacuo at Room-Temperature. *Materials Science and Engineering A*, 1989, **118**, 83-95. DOI: 10.1016/0921-5093(89)90060-9
- [24] VOGT, J. B., J. FOCT, C. REGNARD, G. ROBERT AND J. DHERS. Low-Temperature Fatigue of 316L and 316In Austenitic Stainless-Steels. *Metallurgical Transactions A*, 1991, **22**(10), 2385-2392. DOI: 10.1007/BF02665004
- [25] KRUMML, T., J. POLÁK, K. OBRTLÍK AND S. DEGALLAIX. Dislocation structures in the bands of localised cyclic plastic strain in austenitic 316L and austenitic-ferritic duplex stainless steels. *Acta Materialia*, 1997, **45**(12), 5145-5151. DOI: 10.1016/S1359-6454(97)00178-X
- [26] ANTONOPOULOS, J. G., L. M. BROWN AND A. T. WINTER. Vacancy Dipoles in Fatigued Copper. *Philosophical Magazine A*, 1976, **34**(4), 549-563. DOI : 10.1080/14786437608223793
- [27] BROWN L.M. AND S. L. OGIN. Role of internal stresses in the nucleation of fatigue cracks. In M.K.J. BILBY B.A., WILLIS J.R. ed. *Fundamentals of Deformation and Fracture*. Cambridge University Press, 1985, p. 501-528.
- [28] TANAKA, K. AND T. MURA. A Dislocation Model for Fatigue Crack Initiation. *Journal of Applied Mechanics*, 1981, **48**(1), 97-103. DOI: 10.1115/1.3157599
- [29] ESSMANN, U., U. GOSELE AND H. MUGHRABI. A Model of Extrusions and Intrusions in Fatigued Metals I. Point-Defect Production and the Growth of Extrusions. *Philosophical Magazine A*, 1981, **44**(2), 405-426. DOI: 10.1080/01418618108239541
- [30] POLÁK, J. AND J. MAN. Fatigue crack initiation - The role of point defects. *International Journal of Fatigue*, 2014, **65**, 18-27. DOI: 10.1016/j.ijfatigue.2013.10.016
- [31] BOETTNER, R. C., A. J. MCEVILY AND Y. C. LIU. On the formation of fatigue cracks at twin boundaries. *Philosophical Magazine A*, 1964, **10**(103), 95-106. DOI: 10.1080/14786436408224210

- [32] LLANES, L. AND C. LAIRD. The Role of Annealing Twin Boundaries in the Cyclic Deformation of FCC Materials. *Materials Science and Engineering A*, 1992, **157**(1), 21-27. DOI: 10.1016/0921-5093(92)90094-H
- [33] BLOCHWITZ, C. AND W. TIRSCHLER. Influence of texture on twin boundary cracks in fatigued austenitic stainless steel. *Materials Science and Engineering A*, 2003, **339**(1-2), 318-327. DOI: 10.1016/S0921-5093(02)00126-0
- [34] KAMAYA, M. Influence of bulk damage on crack initiation in low-cycle fatigue of 316 stainless steel. *Fatigue & Fracture of Engineering Materials & Structures*, 2010, **33**(2), 94-104. DOI: 10.1111/j.1460-2695.2009.01420.x
- [35] NEUMANN, P. Analytical solution for the incompatibility stresses at twin boundaries in cubic crystals. *Fatigue '99: Proceedings of the Seventh International Fatigue Congress*, **1/4**, 1999, 107-114.
- [36] WINTER, A. T. Etching Studies of Dislocation Microstructures in Crystals of Copper Fatigued at Low Constant Plastic Strain Amplitude. *Philosophical Magazine*, 1973, **28**(1), 57-64. DOI: 10.1080/14786437308217433
- [37] HEINZ, A. AND P. NEUMANN. Crack Initiation during High Cycle Fatigue of an Austenitic Steel. *Acta Metallurgica et Materialia*, 1990, **38**(10), 1933-1940. DOI: 10.1016/0956-7151(90)90305-Z
- [38] BLOCHWITZ, C., R. RICHTER, W. TIRSCHLER AND K. OBRTLICK The effect of local textures on microcrack propagation in fatigued f.c.c. metals. *Materials Science and Engineering A*, 1997, **234-236**, 563-566. DOI: 10.1016/S0921-5093(97)00320-1
- [39] KIM, W. H. AND C. LAIRD. Crack Nucleation and Stage-I Propagation in High Strain Fatigue - II. Mechanism. *Acta Metallurgica*, 1978, **26**(5), 789-799. DOI: 10.1016/0001-6160(78)90029-9
- [40] CHRIST, H. J. On the orientation of cyclic-slip-induced intergranular fatigue cracks in face-centred cubic metals. *Materials Science and Engineering A*, 1989, **117**, L25-L29. DOI: 10.1016/0921-5093(89)90115-9
- [41] FORSYTH, P. J. A two stage process of fatigue crack growth. In *Symposium Crack Propagation*. College of Aeronautics: Cranfield, U.K., 1961, vol. **II**, p. 76.
- [42] LINDSTEDT, U., B. KARLSSON AND M. NYSTR. Small Fatigue Cracks in an Austenitic Stainless Steel. *Fatigue & Fracture of Engineering Materials & Structures*, 1998, **21**(1), 85-98. DOI: 10.1046/j.1460-2695.1998.00476.x
- [43] ZHIXUE, W. Short fatigue crack parameters describing the lifetime of unnotched steel specimens. *International Journal of Fatigue*, 2001, **23**(4), 363-369. DOI: 10.1016/S0142-1123(00)00101-8
- [44] ZHAO, GAO AND WANG. Interaction and evolution of short fatigue cracks. *Fatigue & Fracture of Engineering Materials & Structures*, 1999, **22**(6), 459-467. DOI: 10.1046/j.1460-2695.1999.00195.x
- [45] KRUPP, U., H. KNOBBE, H. J. CHRIST, P. KOSTER AND C. P. FRITZEN. The significance of microstructural barriers during fatigue of a duplex steel in the high- and very-high-cycle-fatigue (HCF/VHCF) regime. *International Journal of Fatigue*, 2010, **32**(6), 914-920. DOI: 10.1016/j.ijfatigue.2009.09.010
- [46] POLÁK, J. AND P. LIŠKUTÍN. Nucleation and short crack growth in fatigued polycrystalline copper. *Fatigue and Fracture of Engineering Materials and Structures*, 1990, **13**(2), 119-133. DOI: 10.1111/j.1460-2695.1990.tb00584.x
- [47] TRÁVNÍČEK, L., V. MAZÁNOVÁ, J. POLÁK, J. PODUŠKA, L. NÁHLÍK AND P. HUTAŘ. Estimation of short fatigue crack growth rate and residual fatigue life prediction of austenitic Sanicro 25 stainless steel. *Submitted for publication*.

- [48] RITCHIE, R. O. AND J. O. PETERS. Small Fatigue Cracks: Mechanics, Mechanisms and Engineering Applications. *Materials Transactions*, 2001, **42**(1), 58-67. DOI: 10.2320/matertrans.42.58
- [49] RICE, J. R. A path independent integral and the approximate analysis of strain concentrations by notches and cracks. *Journal of Applied Mechanics-Transactions of the ASME*, 1968, **35**, 379-386. DOI : 10.1115/1.3601206
- [50] HUTAŘ, P., J. PODUŠKA, M. ŠMÍD, I. KUBĚNA, A. CHLUPOVÁ, L. NÁHLÍK, J. POLÁK AND T. KRUMML. Short fatigue crack behaviour under low cycle fatigue regime. *International Journal of Fatigue*, 2017, **103**, 207-215. DOI: 10.1016/j.ijfatigue.2017.06.002
- [51] POLÁK, J. Plastic strain-controlled short crack growth and fatigue life. *International Journal of Fatigue*, 2005, **27**(10-12), 1192-1201. DOI: 10.1016/j.ijfatigue.2005.06.028
- [52] COFFIN, L. F. A study of the effects of cyclic thermal stresses on a ductile metal. *Transactions of the ASME*, 1954, **76**, 931-950.
- [53] MANSON, S. S. Behavior of Materials Under Conditions of Thermal Stress. *National Advisory Committee for Aeronautics: Report no. 1170*, Cleveland, 1954.
- [54] POLÁK, J. AND P. ZEZULKA. Short crack growth and fatigue life in austenitic-ferritic duplex stainless steel. *Fatigue & Fracture of Engineering Materials & Structures*, 2005, **28**(10), 923-935. DOI: 10.1111/j.1460-2695.2005.00936.x
- [55] HECZKO, M., J. POLAK AND T. KRUMML. Microstructure and dislocation arrangements in Sanicro 25 steel fatigued at ambient and elevated temperatures. *Materials Science and Engineering A*, 2017, **680**, 168-181. DOI: 10.1016/j.msea.2016.10.076
- [56] GERLAND, M., R. ALAIN, B. A. SAADI AND J. MENDEZ. Low cycle fatigue behaviour in vacuum of a 316L-type austenitic stainless steel between 20 and 600 degrees C. Part II: Dislocation structure evolution and correlation with cyclic behaviour. *Materials Science and Engineering A*, 1997, **229**(1-2), 68-86. DOI: 10.1016/S0921-5093(96)10560-8
- [57] HECZKO, M., B. D. ESSER, T. M. SMITH, P. BERAN, V. MAZÁNOVÁ, D. W. MCCOMB, T. KRUMML, J. POLÁK AND M. J. MILLS. Atomic resolution characterization of strengthening nanoparticles in a new high-temperature-capable 43Fe-25Ni-22.5Cr austenitic stainless steel. *Materials Science and Engineering A*, 2018, **719**, 49-60. DOI: 10.1016/j.msea.2018.02.004
- [58] TRILLO, E. A. AND L. E. MURR. A TEM investigation of M23C6 carbide precipitation behaviour on varying grain boundary misorientations in 304 stainless steels. *Journal of Materials Science*, 1998, **33**(5), 1263-1271. DOI: 10.1023/A:1004390029071
- [59] ROTHMAN, S. J., L. J. NOWICKI AND G. E. MURCH. Self-diffusion in austenitic Fe-Cr-Ni alloys. *Journal of Physics F: Metal Physics*, 1980, **10**, 383-398. DOI: 10.1088/0305-4608/10/3/009
- [60] PETRÁŠ, R. AND J. POLÁK. Damage mechanism in austenitic steel during high temperature cyclic loading with dwells. *International Journal of Fatigue*, 2018, **113**, 335-344. DOI: 10.1016/j.ijfatigue.2018.02.017
- [61] NEUMANN, P. The geometry of slip processes at a propagating fatigue crack - II. *Acta Metallurgica*, 1974, **22**(9), 1167-1178. DOI: 10.1016/0001-6160(74)90072-8

## 7. Veronika Mazánová - List of publications

- [1] MAZÁNOVÁ, V., M. HECZKO, V. ŠKORÍK, A. CHLUPOVÁ, J. POLÁK and T. KRUMML: Microstructure and martensitic transformation in 316L austenitic steel during multiaxial low cycle fatigue at room temperature, *Material Science and Engineering A*. 2019, **767**, 138407
- [2] MAZÁNOVÁ, V., M. HECZKO and J. POLÁK: Fatigue crack initiation and growth in 43Fe-25Ni-22.5Cr austenitic stainless steel at a temperature of 700°C, *International Journal of Fatigue*. 2018, **114**, 11-21.
- [3] MAZÁNOVÁ V. and J. POLÁK: Initiation and short crack growth in austenitic Sanicro 25 steel under the LCF conditions at room temperature. *Fatigue Fracture of Engineering Materials and Structures*. 2018, **41**(7), 1529-1545.
- [4] HECZKO, M., B.D. ESSER, T.M. SMITH, P. BERAN, V. MAZÁNOVÁ, D.W. MCCOMB, T. KRUMML, J. POLÁK and M.J. MILLS: Atomic resolution characterization of strengthening nanoparticles in a new high-temperature-capable 43Fe-25Ni-22.5Cr austenitic stainless steel, *Materials Science & Engineering A*. 2018, **719**, 49-60.
- [5] HECZKO, M., B.D. ESSER, T.M. SMITH, P. BERAN, V. MAZÁNOVÁ, T. KRUMML, J. POLÁK and M.J. MILLS: On the origin of extraordinary cyclic strengthening of the austenitic stainless steel Sanicro 25 during fatigue at 700°C, *Journal of Materials Research*. 2017, **32**(23), 4342-4353.
- [6] POLÁK, J., V. MAZÁNOVÁ, M. HECZKO, R. PETRÁŠ, I. KUBĚNA, L. CASALENA and J. MAN: The role of extrusions and intrusions in fatigue crack initiation, *Engineering Fracture Mechanics*. 2017, **185**, 46-60.
- [7] MAZÁNOVÁ V., V. ŠKORÍK, T. KRUMML and J. POLÁK, Cyclic response and early damage evolution in multiaxial cyclic loading of 316L austenitic steel, *International Journal of Fatigue*. 2017, **100**, 466-476.
- [8] POLÁK, J., V. MAZÁNOVÁ, M. HECZKO, I. KUBĚNA and J. MAN: Profiles of persistent slip markings and internal structure of underlying persistent slip bands, *Fatigue & Fracture of Engineering Materials & Structures*. 2017, **40**(7), 1101-1116.
- [9] POLÁK, J., V. MAZÁNOVÁ, I. KUBĚNA, M. HECZKO and J. MAN: Surface relief and internal structure in fatigued stainless Sanicro 25 steel, *Metallurgical and Materials Transactions A*. 2016, **47**(5), 1907-1911.
- [10] POLÁK J., R. PETRÁŠ and V. MAZÁNOVÁ: Basic mechanisms leading to fatigue failure of structural materials, *Transactions of the Indian Institute of Metals*. 2016 **69**(2), 289-294.

## 8. Curriculum Vitae

**Veronika Mazánová**

(\* December 10, 1989)

mazanova@ipm.cz

ORCID ID: 0000-0002-6804-2632

ResearcherID: B-1028-2017

Scopus Author ID: 57004902800

### EDUCATION

---

<b>Brno University of Technology</b> , Faculty of Mechanical Engineering & <b>Institute of Physics of Materials AS CR</b> PhD Physical and Materials Engineering ( <i>expected</i> )	<b>Brno, Czech Republic</b>  Sep 2014 – 2019
<b>Slovak University of Technology</b> , Faculty of Mechanical Engineering  MS Applied mechanics (Ing.) BS Mechanics (Bc.)	<b>Bratislava, Slovakia</b>  Sep 2012 – Jun 2014 Sep 2009 – Jun 2012

### RESEARCH EXPERIENCE

---

<b>Institute of Physics of Materials AS CR</b> PhD Student <b>Advisor:</b> Prof. Jaroslav Polák, Prof. Tomáš Kruml	<b>Brno, Czech Republic</b> Aug 2014 - Present
<b>Paul Scherrer Institute, Laboratory for Nuclear Materials</b> Visiting Researcher <b>Advisor:</b> Prof. Philippe Spätig	<b>Villigen, Switzerland</b> Feb 2018 – Jul 2018
<b>Slovak University of Technology, Faculty of Mechanical Engineering</b> MS Student <b>Advisor:</b> Ing. Vladimír Chmelko, Ph.D	<b>Bratislava, Slovakia</b> Sep 2012 – Jun 2014

### TEACHING EXPERIENCES

---

<b>Presenter and lecturer</b>  Introduction to Materials Science and Engineering Structure and Properties of Materials Production Technologies	<b>Brno University of Technology</b>  Nov 2014 – Jul 2017 Nov 2014 – Jul 2017 Nov 2014 – Jul 2017
--	---

### CONFERENCE SPEAKING ENGAGEMENTS

---

18th International Conference on the Strength of Material	<i>Columbus, OH, USA</i> Jul 2018
Symposium on Multi-Scale Fatigue, Fracture and Damage in Materials in Harsh Environments	<i>Galway, Ireland</i> Aug 2017
International Colloquium Mechanical Fatigue of Metals	<i>Gijón, Spain</i> Sep 2016
Microscopy & Microanalysis 2016	<i>Columbus, OH, USA</i> Jul 2016
International Conference on Multiaxial Fatigue and Fracture 11	<i>Seville, Spain</i> Jun 2016
Materials Structure & Micromechanics of Fracture 8	<i>Brno, Czech Republic</i> Jun 2016
27th Colloquium on Fatigue Mechanisms	<i>Vienna, Austria</i> Mar 2016
International Conference on Mechanical Behavior of Materials 12	<i>Karlsruhe, Germany</i> May 2015

**Abstract:** Advanced highly-alloyed austenitic stainless steel Sanicro 25 was studied under the conditions of low cycle fatigue at room temperature and at elevated temperature of 700°C. Several state-of-the-art experimental techniques were used to investigate the mutual effects of alloy composition, microstructural changes and deformation mechanisms, which determine the overall damage resistance of the material. The main effort has been focused on the fatigue crack initiation and the short crack growth.

- The internal deformation mechanisms were correlated with the evolution of the surface relief in the form of persistent slip markings. It was found that the high planar character of the dislocation slip causes the high cyclic plastic strain localization into the persistent slip bands and thus the early Stage I crack nucleation associated with the presence of the persistent slip markings in all studied samples. The twin boundary cracking was found to be related to the presence of the persistent slip marking along the surface trace of twin boundary as well. The intergranular crack initiation was observed only rarely at high strain amplitude loading.
- The crack growth rates of the longest cracks were measured on the samples with a shallow notch. The results were analysed using the fracture mechanics approaches based both on amplitude of  $K_I$  and of  $J$ -integral as well as on the plastic strain amplitude. All approaches were discussed in the relation to the Manson-Coffin fatigue life curve.
- In the case of cycling at elevated temperature the role of oxidation was studied. The brittle cracking of the oxidized grain boundaries was found to play a major role in the early stages of crack nucleation. Later the crack growth path changes to be preferentially transgranular. The crack growth path is very similar to that studied in room temperature cycling.

**Abstrakt:** Pokročilá vysoce legovaná austenitická nerezová ocel Sanicro 25 byla studována za podmínek nízkocyklové únavy za pokojové a vysoké teploty 700°C. Široká škála moderních experimentálních technik byla použita ke studiu vzájemně souvisejících efektů chemického složení slitiny, mikrostrukturních změn a deformačních mechanismů, které určují odolnost materiálu vůči poškození. Hlavní úsilí bylo zaměřeno na studium iniciace únavových trhlin a růstu krátkých trhlin.

- Vnitřní deformační mechanismy byly korelovány s vývojem povrchového reliéfu, který je pozorován ve formě persistentních skluzových stop na povrchu. Bylo zjištěno, že vysoce planární charakter dislokačního skluzu způsobuje vysokou lokalizaci cyklické plastické deformace do persistentních skluzových pásů, což v důsledku vede k nukleaci "Stage I" trhlin, která je spojena s přítomností persistentních skluzových stop na povrchu ve všech studovaných vzorcích. Bylo zjištěno, že praskání dvojčatových hranic je také spojeno s přítomností persistentních skluzových stop podél povrchové stopy dvojčatové roviny. Interkrystalická iniciace únavové trhliny byla pozorována pouze zřídka, a to za podmínek zatěžování amplitudami vysoké deformace.
- Rychlosti šíření nejdelších trhlin byly měřeny na vzorcích s mělkým vrubem. Výsledky byly analyzovány použitím přístupů lomové mechaniky založených na amplitudě  $K_I$  a  $J$ -integrálu stejně jako na amplitudě plastické deformace. Všechny přístupy byly diskutovány v souvislosti s Mansonovými-Coffinovými křivkami únavové životnosti.
- Byla studována role oxidace v podmínkách cyklického zatěžování za vysokých teplot. Bylo zjištěno, že křehké praskání zoxidovaných hranic zrn hraje hlavní roli v počátečních stádiích nukleace trhlin. Později po iniciaci se dráha růstu trhliny mění preferenčně na transkrystalickou. Dráha šíření trhlin je velmi podobná dráze zjištěné při cyklování za pokojové teploty.